

Combustion synthesis and characterization of visible-light-driven La/Al co-doped ZnO nanoparticles used for wastewater treatment

A. Phuruangrat^{a,*}, T. Thongtem^{b,c}, S. Thongtem^{b,d}

^a*Division of Physical Science, Faculty of Science, Prince of Songkla University, Hat Yai, Songkhla 90112, Thailand*

^b*Materials Science Research Center, Faculty of Science, Chiang Mai University, Chiang Mai 50200, Thailand*

^c*Department of Chemistry, Faculty of Science, Chiang Mai University, Chiang Mai 50200, Thailand*

^d*Department of Physics and Materials Science, Faculty of Science, Chiang Mai University, Chiang Mai 50200, Thailand*

Visible-light-driven $\text{La}_x\text{Al}_{0.03-x}\text{Zn}_{0.97}\text{O}$ ($x = 0.01, 0.015$ and 0.02) nanoparticles were synthesized by tartaric acid-assisted combustion method. Both ZnO and La/Al co-doped ZnO samples were indexed to the pure hexagonal wurtzite ZnO structure and were composed of nanoparticles with particle size ranges of 100-150 nm and 20-50 nm, respectively. The photocatalytic activities of ZnO and $\text{La}_x\text{Al}_{0.03-x}\text{Zn}_{0.97}\text{O}$ ($x = 0.01, 0.015$ and 0.02) nanoparticles were monitored through the degradation of methylene blue (MB) under visible light irradiation. The $\text{La}_{0.02}\text{Al}_{0.01}\text{Zn}_{0.97}\text{O}$ nanoparticles have the highest photocatalytic activity in degrading of MB under visible light irradiation because the La/Al co-dopant played the role in creating shallow energy level under the conduction band of ZnO.

(Received August 6, 2023; Accepted November 17, 2023)

Keywords: La/Al co-doped ZnO nanoparticles, Combustion method, Photocatalysis

1. Introduction

In recent years, environmental pollution caused by dyes containing in wastewater is a serious problem that influences on health and hygiene of aquatic and non-aquatic organisms [1-4]. Semiconductor-based photocatalysts such as TiO_2 [5, 6], ZnO [2, 7, 8], CuO [9, 10] and Fe_2O_3 [11, 12] have high efficiency in transforming toxic organic compounds into non-toxic components. They are inexpensive with physical and chemical stability, high oxidative capacity and reusability [4, 13, 14]. ZnO with a wide band-gap II-VI semiconductor of 3.37 eV and exciton binding energy of 60 meV is a promising material used for optoelectronic, magnetic and energy harvesting applications for solar cells, photo detectors and transparent conductive films [1, 4, 7, 15, 16]. ZnO has the promising photodegradation of dyes such as methylene blue (MB) [2, 8, 7], rhodamine B (RhB) [17, 18], methyl orange (MO) [19, 20] and malachite green (MG) [21, 22] because of its nontoxic, abundant, low cost, structural stability and environmentally friendly [4, 7, 23]. The photocatalytic reaction of ZnO is active only UV light region due to its wide band gap and high rate of electron-hole recombination [4, 13, 23, 24]. To solve this problem, a metallic dopant is added to respond visible light with 45% of the solar radiation because the metal dopant can be tuned with its optical band gap energy which can lead to enhance the carrier-charge separation by creating traps for electrons. Additionally, metal co-doped ZnO has the photocatalytic performance higher than single metal doped ZnO because the co-dopant can lead to effectively separate the photo-induced charge carriers with strong visible light harvesting [25-29]. Reddy et al. reported that 2%Al-2%Ni-ZnO nanoparticles are very effective for the degradation of MO under visible

* Corresponding author: phuruangrat@hotmail.com
<https://doi.org/10.15251/DJNB.2023.184.1423>

radiation within 30 min [25]. Nibret et al. reported the successful synthesis of Cr/N co-doped ZnO nanoparticles used for the degradation of thymol blue under visible light [28]. Cr/N co-doped ZnO has photocatalytic efficiency higher than ZnO, N-doped ZnO and Cr-doped ZnO nanoparticles because of the synergistic effect of co-dopant. Irtiqa and Rahman reported the successful synthesis of Ce/Dy co-doped ZnO nanoparticles by simple co-precipitation method [29]. The photocatalytic performance of Ce_{0.05}Dy_{0.05}Zn_{0.90}O nanoparticles in degrading of RhB was improved by the increase of surface oxygen vacancy and absorption capacity and the delay of photo-generated electron-hole recombination.

In this research, ZnO and La_xAl_{0.03-x}Zn_{0.97}O (x = 0.01, 0.015 and 0.02) nanoparticles were synthesized by tartaric acid-assisted combustion method. Structure, morphology and optical property of ZnO and La_xAl_{0.03-x}Zn_{0.97}O (x = 0.01, 0.015 and 0.02) nanoparticles were characterized by X-ray diffraction (XRD), transmission electron microscopy (TEM), Fourier transform infrared spectroscopy (FTIR), Raman spectroscopy and UV-visible spectrometry. The photocatalytic properties of ZnO and La_xAl_{0.03-x}Zn_{0.97}O (x = 0.01, 0.015 and 0.02) nanoparticles were tested through the degradation of methylene blue (MB) as a dye model under visible radiation.

2. Experimental details

To prepare La_xAl_{0.03-x}Zn_{0.97}O (x = 0.01, 0.015 and 0.02) nanoparticles, La(NO₃)₃·6H₂O, Al(NO₃)₃·9H₂O and Zn(NO₃)₂·6H₂O were used as La, Al and Zn sources. First, 0.01 mole of Zn(NO₃)₂·6H₂O was dissolved in 25 ml of ethanol under continual stirring. Second, 0.01-0.02 wt% of La(NO₃)₃·6H₂O and Al(NO₃)₃·9H₂O were dissolved in 25 ml of ethanol which was added to the Zn²⁺ solution. Third, 0.01 mole of tartaric acid in 50 ml ethanol and 0.001 mole of NaOH in 50 ml ethanol were added in the mixed solution to form white gel under magnetic stirring for 24 h. The as-synthesized white gel was filtered, washed with deionized water and ethanol, and dried at 80 °C for 24 h. The dried precursor was ground in an alumina crucible and calcined in an electric furnace at 600 °C for 4 h to obtain the final La_xAl_{0.03-x}Zn_{0.97}O (x = 0.01, 0.015 and 0.02) samples. Similarly, the process was done for the synthesis of ZnO.

Phase and structure of ZnO and La/Al co-doped ZnO samples were characterized by X-ray diffraction (XRD) on a Philips X'Pert MPD X-ray diffractometer equipped with Cu-K_α radiation at a scanning rate of 0.02 deg/s over the range of 20° - 80°. The morphologies of ZnO and La/Al co-doped ZnO samples were recorded by a transmission electron microscope (TEM JEM 2010, JEOL) at an acceleration voltage of 200 kV. The Fourier transform infrared (FTIR) and Raman spectra of ZnO and La/Al co-doped ZnO samples were recorded by Bruker TENSOR 27 Fourier transform infrared spectroscopy with KBr as a diluting agent and HORIBA JOBIN YVON T64000 Raman spectroscopy using 30 mW He-Ne laser with 632.8 nm wavelength. The optical properties of ZnO and La/Al co-doped ZnO samples were investigated by a UV-visible spectrometer (Lambda 25 Perkin Elmer) with 0.2 nm resolution at ~225-800 nm wavelength.

The photocatalytic activities of ZnO and La/Al co-doped ZnO samples were investigated through the degradation of methylene blue (MB) as a dye model under visible radiation. Each 200 mg photocatalyst was added in 200 ml 1×10⁻⁵ M MB aqueous solution which was magnetically stirred in the dark for 30 min. Then visible light from a 35 W xenon lamp was illuminated on the solution system and the suspension solution was collected every 30 min interval. The concentration of MB was analyzed by Lambda 25 UV-visible spectroscopy (Perkin Elmer) at a maximum wavelength (λ_{max}) of 664 nm. The decolorization efficiency (%) was calculated by

$$\text{Decolorization efficiency (\%)} = \frac{C_o - C_t}{C_o} \times 100 \quad (1)$$

C_o and C_t are the concentrations of MB before and after visible light illumination.

3. Results and discussion

XRD patterns of ZnO and $\text{La}_x\text{Al}_{0.03-x}\text{Zn}_{0.97}\text{O}$ ($x = 0.01, 0.015$ and 0.02) samples prepared by combustion method and followed by calcination at $600\text{ }^\circ\text{C}$ for 4 h are shown in Fig. 1. The XRD pattern of pure ZnO sample can be indexed to the hexagonal wurtzite ZnO structure (JCPDS no. 36-1451 [30]). It presents the diffraction peaks at 2θ of $31.86^\circ, 34.47^\circ, 36.37^\circ, 47.67^\circ, 56.68^\circ, 62.92^\circ, 66.35^\circ, 68.01^\circ, 69.13^\circ, 72.55^\circ$ and 77.02° which correspond to the (100), (002), (101), (102), (110), (103), (200), (112), (201), (004) and (202) crystallographic planes of hexagonal wurtzite ZnO structure. Comparing to the XRD pattern of ZnO, the XRD patterns of $\text{La}_x\text{Al}_{0.03-x}\text{Zn}_{0.97}\text{O}$ ($x = 0.01, 0.015$ and 0.02) contain eleven diffraction peaks in the same way as that of pure ZnO sample. They indicate that the La/Al co-dopants did not play the role in changing the hexagonal wurtzite ZnO structure [14, 15, 24, 26]. The diffraction peaks of $\text{La}_x\text{Al}_{0.03-x}\text{Zn}_{0.97}\text{O}$ ($x = 0.01, 0.015$ and 0.02) were broadened because La/Al co-dopants have the influence to suppress the growth of ZnO crystal by the substitution of La/Al co-dopants for Zn^{2+} sites of ZnO lattice [14, 15, 24, 26].

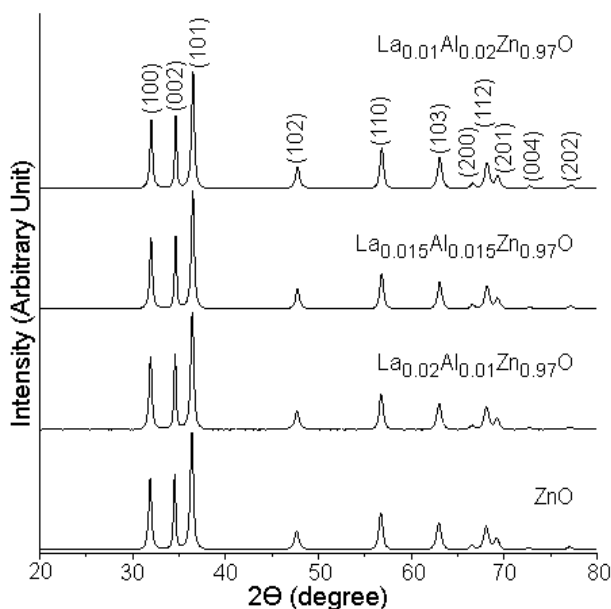


Fig. 1. XRD patterns of ZnO and La/Al co-doped ZnO samples prepared by combustion method and followed by calcination at $600\text{ }^\circ\text{C}$ for 4 h.

The crystallite sizes of ZnO, $\text{La}_{0.01}\text{Al}_{0.02}\text{Zn}_{0.97}\text{O}$, $\text{La}_{0.015}\text{Al}_{0.015}\text{Zn}_{0.97}\text{O}$ and $\text{La}_{0.02}\text{Al}_{0.01}\text{Zn}_{0.97}\text{O}$ samples calculated by the Scherrer equation were 48.32, 28.95, 26.59 and 23.25 nm, respectively [7, 14, 18, 21, 22]. The specific surface areas (SSA) of the samples were calculated by

$$\text{SSA} = K_{\text{sf}}/D \cdot \rho \quad (2)$$

K_{sf} is the spherical shape factor for nanoparticles ($K_{\text{sf}} = 6$), D is the crystallite size and ρ is the density of ZnO ($5.606\text{ g}\cdot\text{cm}^{-3}$) [7, 31, 32]. The specific surface areas were 22.14, 36.97, 40.25 and $46.03\text{ m}^2\cdot\text{g}^{-1}$ for ZnO, $\text{La}_{0.01}\text{Al}_{0.02}\text{Zn}_{0.97}\text{O}$, $\text{La}_{0.015}\text{Al}_{0.015}\text{Zn}_{0.97}\text{O}$ and $\text{La}_{0.02}\text{Al}_{0.01}\text{Zn}_{0.97}\text{O}$ samples, respectively. Clearly, the specific surface area of La/Al co-doped ZnO is higher than that of pure ZnO sample. This is the benefit of increasing in the number of surface active sites and enhancing the photocatalytic performance of ZnO [7, 20, 28, 31].

Fig. 2a shows the FTIR spectra of Zn-tartaric acid precursor, ZnO and $\text{La}_{0.015}\text{Al}_{0.015}\text{Zn}_{0.97}\text{O}$ samples prepared by the combustion method. FTIR spectrum of La/Al co-doped ZnO-tartaric acid precursor shows the functional carboxyl groups of tartaric acid as bidentate ligand at $1500\text{--}1800\text{ cm}^{-1}$ and $1200\text{--}1450\text{ cm}^{-1}$ by donating of the lone pair electron to form inorganic metal-tartaric

complexes [7, 14, 31, 33]. Upon calcination the precursor at 600 °C for 4 h, the vibration of functional groups of tartaric acid was no longer detected in the FTIR spectra of ZnO and $\text{La}_{0.015}\text{Al}_{0.015}\text{Zn}_{0.97}\text{O}$ samples. The results indicate that the crystalline samples were completely produced [7, 14]. The FTIR spectrum of ZnO shows a new strong absorption band at 421 cm^{-1} ascribed to the Zn–O stretching vibration [2, 4, 7, 8]. The wavenumber of Zn–O stretching vibration was shifted from 421 cm^{-1} for ZnO to 423 cm^{-1} for $\text{La}_{0.015}\text{Al}_{0.015}\text{Zn}_{0.97}\text{O}$ caused by the change of bond length of Zn–O by the La/Al dopant. Thus, La/Al co-dopant was substituted for Zn^{2+} sites of ZnO lattice [15, 34, 35]. In addition, ZnO and $\text{La}_{0.015}\text{Al}_{0.015}\text{Zn}_{0.97}\text{O}$ sample show a broad band at $3050\text{--}3650\text{ cm}^{-1}$ corresponding to the O–H stretching of adsorbed water on the top [2, 4, 7, 8].

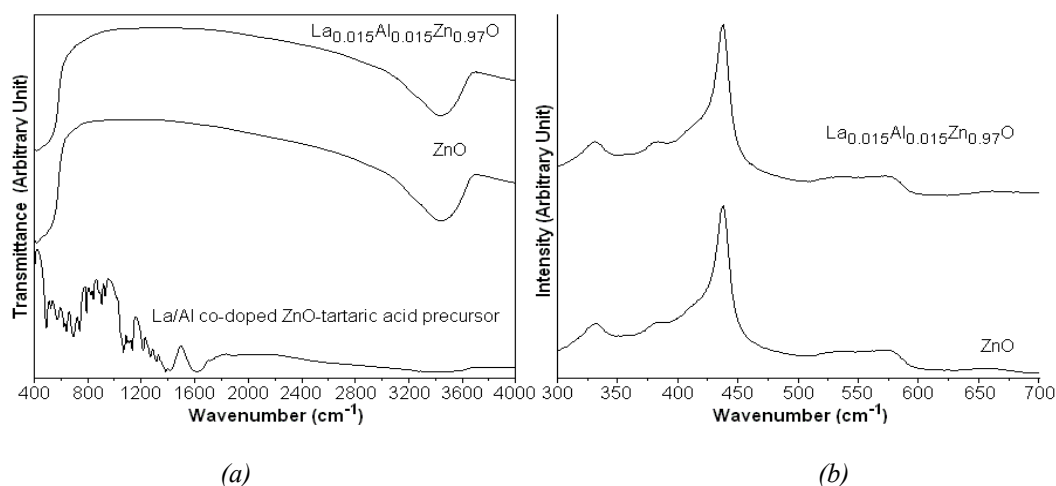


Fig. 2. (a) FTIR and (b) Raman spectra of precursor, ZnO and $\text{La}_{0.015}\text{Al}_{0.015}\text{Zn}_{0.97}\text{O}$ samples prepared by combustion method.

Fig. 2b shows the Raman spectra of ZnO and $\text{La}_{0.015}\text{Al}_{0.015}\text{Zn}_{0.97}\text{O}$ samples prepared by combustion method and followed by calcination at 600 °C for 4 h. The characteristic sharp Raman peak at 437 cm^{-1} was detected in pure hexagonal wurtzite ZnO sample which corresponds to the non-polar optical phonon E_{2H} mode [1, 2, 7, 8, 16]. They should be noted that the E_{2H} mode of $\text{La}_{0.015}\text{Al}_{0.015}\text{Zn}_{0.97}\text{O}$ sample was broadened and shifted to 435 cm^{-1} and that the lattice of ZnO was distorted by the effective substitution for Zn^{2+} ion by La/Al co-dopant [15, 34, 35]. The $E_{2H} - E_{2L}$ (multi-phonon process) and A_{1T} modes of hexagonal wurtzite ZnO structure were detected at 329 and 380 cm^{-1} [1, 2, 7, 8]. The weak Raman peak at 581 cm^{-1} of hexagonal wurtzite ZnO structure is assigned to the E_1 symmetry with LO mode [1, 2, 7, 8]. In general, the $E_1(\text{LO})$ mode of ZnO is caused by the impurities and defects containing in ZnO lattice such as oxygen vacancy and Zn interstitial [1, 2, 7, 8]. The $E_1(\text{LO})$ mode of $\text{La}_{0.015}\text{Al}_{0.015}\text{Zn}_{0.97}\text{O}$ sample was broadened. Clearly, the La/Al dopant played the role in creating impurities and defects of ZnO lattice [15, 34, 36, 37].

The morphologies of ZnO and $\text{La}_x\text{Al}_{0.03-x}\text{Zn}_{0.97}\text{O}$ ($x = 0.01, 0.015$ and 0.02) samples prepared by combustion method and followed by calcination at 600 °C for 4 h were analyzed by TEM as the results shown in Fig. 3. TEM images of ZnO and $\text{La}_x\text{Al}_{0.03-x}\text{Zn}_{0.97}\text{O}$ ($x = 0.01, 0.015$ and 0.02) show that all samples were composed of spherical nanoparticles with different sizes. The particle size range of ZnO and La/Al co-doped ZnO samples were 100–150 and 20–50 nm, respectively. The average particle sizes of the samples were 127 ± 35 , 46 ± 9 , 33 ± 8 and 30 ± 5 nm for ZnO, $\text{La}_{0.01}\text{Al}_{0.02}\text{Zn}_{0.97}\text{O}$, $\text{La}_{0.015}\text{Al}_{0.015}\text{Zn}_{0.97}\text{O}$ and $\text{La}_{0.02}\text{Al}_{0.01}\text{Zn}_{0.97}\text{O}$, respectively. The particle size of ZnO was decreased because the La/Al co-dopant played the role in reducing growth rate of ZnO nanoparticles. The selected area electron diffraction (SAED) patterns of ZnO and $\text{La}_x\text{Al}_{0.03-x}\text{Zn}_{0.97}\text{O}$ ($x = 0.01, 0.015$ and 0.02) show bright electron diffraction rings which can be indexed to the pure phase of hexagonal wurtzite ZnO structure (JCPDS no. 36-1451) [30].

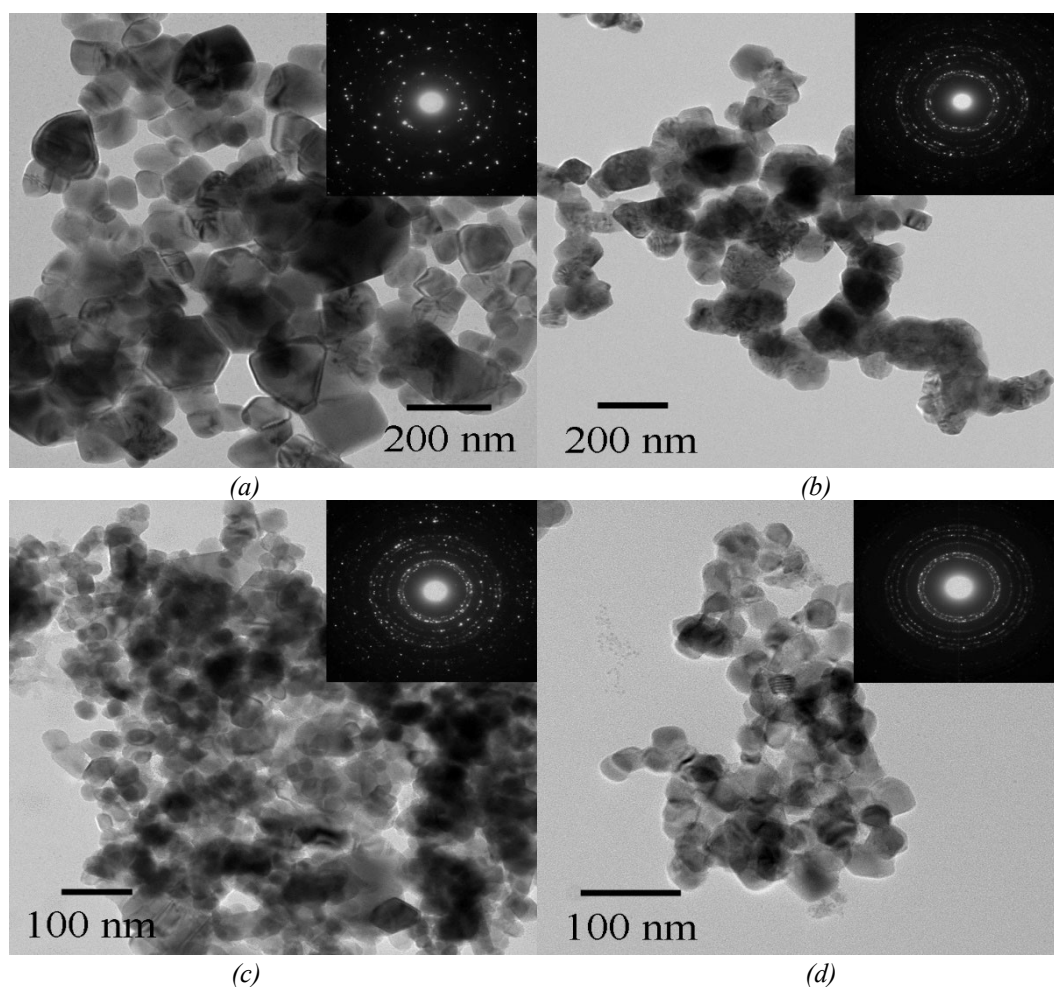


Fig. 3. TEM images and SAED patterns of (a) ZnO, (b) $\text{La}_{0.01}\text{Al}_{0.02}\text{Zn}_{0.97}\text{O}$, (c) $\text{La}_{0.015}\text{Al}_{0.015}\text{Zn}_{0.97}\text{O}$ and (d) $\text{La}_{0.02}\text{Al}_{0.01}\text{Zn}_{0.97}\text{O}$ samples prepared by combustion method and followed by calcination at 600 °C for 4 h.

The optical properties of ZnO and $\text{La}_x\text{Al}_{0.03-x}\text{Zn}_{0.97}\text{O}$ ($x = 0.01, 0.015$ and 0.02) samples prepared by combustion method and followed by calcination at 600 °C for 4 h were investigated by UV-visible absorption spectroscopy as the results shown in Fig. 4. The UV-visible absorption spectrum of pure ZnO nanoparticles shows strong absorption in UV region with absorption edge of 378 nm due to the electronic transition from the valence band (VB) to the conduction band (CB) of ZnO [1, 18, 20]. The absorption in visible region of La/Al co-doped ZnO nanoparticles is higher than that of ZnO nanoparticles. Comparing to ZnO nanoparticles, the absorption edges of $\text{La}_{0.01}\text{Al}_{0.02}\text{Zn}_{0.97}\text{O}$, $\text{La}_{0.015}\text{Al}_{0.015}\text{Zn}_{0.97}\text{O}$ and $\text{La}_{0.02}\text{Al}_{0.01}\text{Zn}_{0.97}\text{O}$ samples were red shifted to 381, 380 and 382 nm, respectively.

Band gap (E_g) of the samples can be calculated by the following.

$$E_g = 1240/\lambda \quad (3)$$

λ is the wavelength (nm) of the adsorption edge [18, 28, 38, 39]. The calculated band gaps were 3.280, 3.255, 3.263 and 3.246 eV for ZnO, $\text{La}_{0.01}\text{Al}_{0.02}\text{Zn}_{0.97}\text{O}$, $\text{La}_{0.015}\text{Al}_{0.015}\text{Zn}_{0.97}\text{O}$ and $\text{La}_{0.02}\text{Al}_{0.01}\text{Zn}_{0.97}\text{O}$ samples, respectively. The E_g of ZnO was decreased by La/Al adding because the La/Al dopant played the role in creating a new energy level in the band gap of ZnO lattice [26, 28, 38]. The added La/Al dopant has the benefit for visible light harvesting of the visible-light driven photocatalyst.

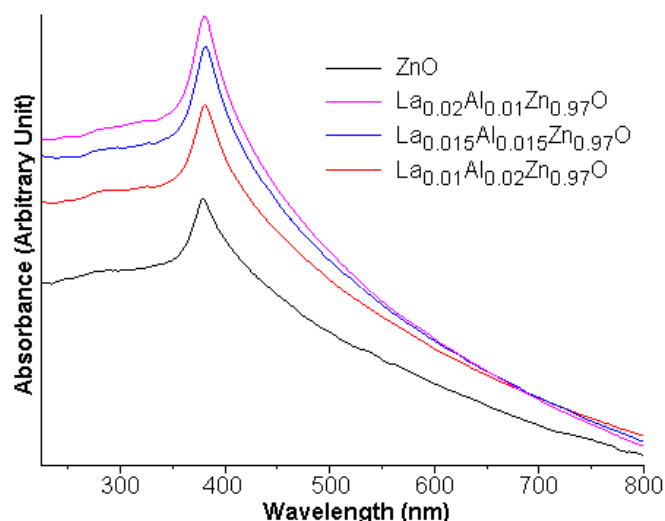


Fig. 4. UV-visible absorption of ZnO and $\text{La}_x\text{Al}_{0.03-x}\text{Zn}_{0.97}\text{O}$ ($x = 0.01, 0.015$ and 0.02) nanoparticles prepared by combustion method and followed calcination at 600°C for 4 h.

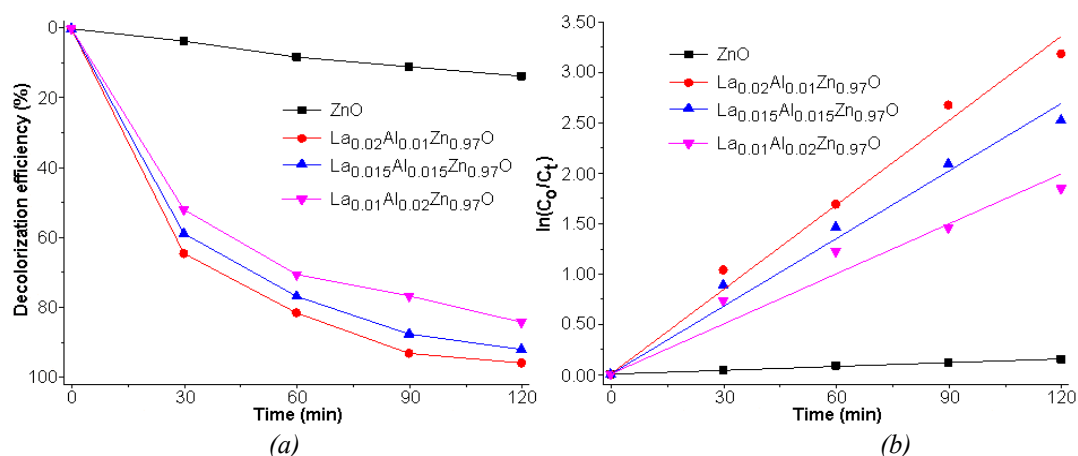


Fig. 5. (a) Photodegradation and (b) $\ln(C_0/C_t)$ versus irradiation time plot of ZnO and La/Al co-doped ZnO nanoparticles prepared by combustion method and followed by calcination at 600°C for 4 h.

The photocatalytic efficiencies of ZnO and $\text{La}_x\text{Al}_{0.03-x}\text{Zn}_{0.97}\text{O}$ ($x = 0.01, 0.015$ and 0.02) nanoparticles prepared by combustion method and followed by calcination at 600°C for 4 h were monitored through the degradation of MB under visible radiation as the results shown in Fig. 5a. The photodegradation efficiency of ZnO nanoparticles was 13.61 % within 120 min because of its wide band gap energy of 3.280 eV. The photodegradation efficiency was increased by La/Al co-dopant adding because the La/Al co-dopant played the role in creating a shallow energy level under the conduction band of ZnO. The photo-excited electrons can be trapped and the photocatalytic performance of ZnO under visible light was enhanced [26, 40, 41]. La ion acts as an electron trapper which can lead to suppress electron-hole recombination [29, 42, 43]. The photodegradation efficiencies of $\text{La}_{0.01}\text{Al}_{0.02}\text{Zn}_{0.97}\text{O}$, $\text{La}_{0.015}\text{Al}_{0.015}\text{Zn}_{0.97}\text{O}$ and $\text{La}_{0.02}\text{Al}_{0.01}\text{Zn}_{0.97}\text{O}$ samples illuminated by visible light within 120 min were 84.16%, 91.98% and 95.86%, respectively. In this research, $\text{La}_{0.02}\text{Al}_{0.01}\text{Zn}_{0.97}\text{O}$ nanoparticles have the highest photocatalytic efficiency and are 7.04 times that of pure ZnO nanoparticles. The degradation rate of MB over ZnO and $\text{La}_x\text{Al}_{0.03-x}\text{Zn}_{0.97}\text{O}$ ($x = 0.01, 0.015$ and 0.02) under visible light irradiation was calculated through the first-order kinetic model as the results shown in Fig. 5b [2, 4, 7, 8]. The photocatalytic

rate constants for MB degradation were 1.24×10^{-3} , 0.0166, 0.0223 and 0.0278 min^{-1} for ZnO, $\text{La}_{0.01}\text{Al}_{0.02}\text{Zn}_{0.97}\text{O}$, $\text{La}_{0.015}\text{Al}_{0.015}\text{Zn}_{0.97}\text{O}$ and $\text{La}_{0.02}\text{Al}_{0.01}\text{Zn}_{0.97}\text{O}$ nanoparticles, respectively. The $\text{La}_{0.02}\text{Al}_{0.01}\text{Zn}_{0.97}\text{O}$ nanoparticles have the highest photocatalytic performance in degrading of MB under visible radiation.

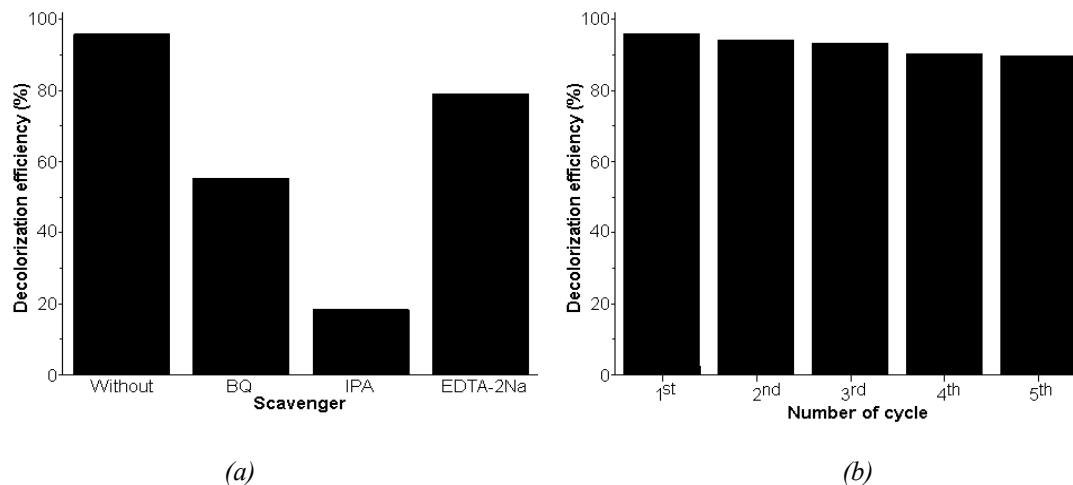


Fig. 6. (a) Trapping experiment with and without different scavengers and (b) recycle test for MB degradation of $\text{La}_{0.02}\text{Al}_{0.01}\text{Zn}_{0.97}\text{O}$ nanoparticles prepared by combustion method and followed by calcination at $600 \text{ }^\circ\text{C}$ for 4 h.

The role of active radicals in degrading MB photocatalyzed by $\text{La}_{0.02}\text{Al}_{0.01}\text{Zn}_{0.97}\text{O}$ nanoparticles was investigated through the trapping experiment using ethylenediaminetetraacetic acid disodium salt (EDTA-2Na), isopropyl alcohol (IPA) and benzoquinone (BQ) for trapping hole (h^+), hydroxyl radical ($\bullet\text{OH}$) and superoxide anion radical ($\bullet\text{O}_2^-$) as the results shown in Fig. 6a [2, 17, 44, 45]. The photodegradation efficiencies of $\text{La}_{0.02}\text{Al}_{0.01}\text{Zn}_{0.97}\text{O}$ nanoparticles were significantly suppressed for IPA and BQ adding, therefore, $\bullet\text{OH}$ and $\bullet\text{O}_2^-$ are the important active radicals used for photodegradation of MB. In addition, the $\text{La}_{0.02}\text{Al}_{0.01}\text{Zn}_{0.97}\text{O}$ nanoparticles show excellent reusability for photocatalytic degradation of MB under visible light for five cycles as the results shown in Fig. 6b. In this research, the $\text{La}_{0.02}\text{Al}_{0.01}\text{Zn}_{0.97}\text{O}$ nanoparticles are the promising candidate for practical photocatalysis in degrading of MB containing in wastewater.

4. Conclusions

In summary, visible-light-driven $\text{La}_x\text{Al}_{0.03-x}\text{Zn}_{0.97}\text{O}$ ($x = 0.01, 0.015$ and 0.02) nanoparticles were synthesized by tartaric acid-assisted combustion method. XRD patterns of ZnO and La/Al co-doped ZnO nanoparticles were indexed to the pure phase of hexagonal wurtzite ZnO structure. TEM images were used to certify uniform nanoparticles with particle sizes of 127 ± 35 , 46 ± 9 , 33 ± 8 and 30 ± 5 nm for ZnO, $\text{La}_{0.01}\text{Al}_{0.02}\text{Zn}_{0.97}\text{O}$, $\text{La}_{0.015}\text{Al}_{0.015}\text{Zn}_{0.97}\text{O}$ and $\text{La}_{0.02}\text{Al}_{0.01}\text{Zn}_{0.97}\text{O}$, respectively. The photocatalytic activities of ZnO and La/Al co-doped ZnO nanoparticles were investigated through the degradation of MB illuminated by visible light. In this research, $\text{La}_{0.02}\text{Al}_{0.01}\text{Zn}_{0.97}\text{O}$ nanoparticles have the highest photocatalytic efficiency in degrading of MB because La/Al co-dopant played the role in suppressing electron-hole recombination during the photocatalytic reaction. The $\text{La}_{0.02}\text{Al}_{0.01}\text{Zn}_{0.97}\text{O}$ nanoparticles have excellent reusability for photocatalysis and are the promising candidate for practical degradation of MB under visible light.

Acknowledgement

This research was supported by National Science, Research and Innovation Fund (NSRF) and Prince of Songkla University (Grant No. SCI6601194S).

References

- [1] T. Mahardika, N.A. Putri, A.E. Putri, V. Fauzia, L. Roza, I. Sugihartono, Y. Herbani, Results Phys. 13, 102209 (2019); <https://doi.org/10.1016/j.rinp.2019.102209>
- [2] A. Phuruangrat, B. Kuntalue, S. Thongtem, T. Thongtem, Optik 226, 165949 (2021); <https://doi.org/10.1016/j.ijleo.2020.165949>
- [3] L. Li, M. Ma, S. Guan, H. Wu, Res. Chem. Intermed. 44, 4365 (2018); <https://doi.org/10.1007/s11164-018-3392-2>
- [4] X. Wu, Y. Zhang, H. Wu, J. Guo, K. Wu, L. Zhang, J. Mater. Sci. 32, 26241 (2021); <https://doi.org/10.1007/s10854-021-06844-z>
- [5] J. Sakfali, S. Ben Chaabene, R. Akkari, M.S. Zina, Russ. J. Inorg. Chem. 67, 1324 (2022); <https://doi.org/10.1134/S003602362208023X>
- [6] S. Kaushal, H. Kaur, S. Kumar, R. Badru, S. Mittal, P. Singh, Russ. J. Inorg. Chem. 65, 616 (2020); <https://doi.org/10.1134/S0036023620040087>
- [7] S. Sa-nguanprang, A. Phuruangrat, T. Thongtem, S. Thongtem, Russ. J. Inorg. Chem. 65, 1102 (2020); <https://doi.org/10.1134/S0036023620070189>
- [8] A. Phuruangrat, S. Thongtem, T. Thongtem, Mater. Design 107, 250 (2016); <https://doi.org/10.1016/j.matdes.2016.06.045>
- [9] C. Saovakon, P. Jansanthea, J. Aust. Ceram. Soc. 56, 1385 (2020); <https://doi.org/10.1007/s41779-020-00488-8>
- [10] H.B. Uma, M.S.V. Kumar, S. Ananda, J. Mol. Struct. 1264, 133110 (2022); <https://doi.org/10.1016/j.molstruc.2022.133110>
- [11] W. Chomkitichai, P. Jansanthea, D. Channei, Russ. J. Inorg. Chem. 66, 1995 (2021); <https://doi.org/10.1134/S0036023621130027>
- [12] A. Saranya, A. Thamer, K. Ramar, A. Priyadharsan, R. Ve, K. Murugan, A. Murad, P. Maheshwaran, J. Photochem. Photobiol. B 207, 111885 (2020); <https://doi.org/10.1016/j.jphotobiol.2020.111885>
- [13] B.M. Rajbongshi, A. Ramchiary, B.M. Jha, S.K. Samdarshi, J. Mater. Sci. 25, 2969 (2014); <https://doi.org/10.1007/s10854-014-1968-1>
- [14] R. Elilarassi, G. Chandrasekaran, Mater. Sci. Semicond. Process. 14, 179 (2011); <https://doi.org/10.1016/j.mssp.2010.11.001>
- [15] K.C. Barick, M. Aslam, V.P. Dravid, D. Bahadur, J Colloid Interf. Sci. 349, 19 (2010); <https://doi.org/10.1016/j.jcis.2010.05.036>
- [16] T. Thongtem, A. Phuruangrat, S. Thongtem, Curr. Appl. Phys. 9, S197 (2009); <https://doi.org/10.1016/j.cap.2009.01.040>
- [17] L.A. Thi, S.Y. Pung, S. Sreekantan, A. Matsuda, H.D. Phu, IOP Conf. Ser.: J. Phys. Conf. Ser. 1082, 012045 (2018); <https://doi.org/10.1088/1742-6596/1082/1/012045>
- [18] S. Rajendrachari, P. Taslimi, A.C. Karaoglanli, O. Uzun, E. Alp, G.K. Jayaprakash, Arabian J. Chem. 14, 103180 (2021); <https://doi.org/10.1016/j.arabjc.2021.103180>
- [19] T. Bi, Z. Du, S. Chen, H. He, X. Shen, Y. Fu, Appl. Surf. Sci. 614, 156240 (2023); <https://doi.org/10.1016/j.apsusc.2022.156240>
- [20] N. Tripathy, R.Ahmad, H. Kuk, D.H. Lee, Y.B. Hahn, G. Khang, J. Photochem. Photobiol. B 161, 312 (2016); <https://doi.org/10.1016/j.jphotobiol.2016.06.003>
- [21] S. Meena, D. Vaya, B.K. Das, Bull. Mater. Sci. 39, 1735 (2016); <https://doi.org/10.1007/s12034-016-1318-4>
- [22] M.A. Bhatti, A. Tahira, A. Chandio, K.F. Almani, A.L. Bhatti, B. Waryani, A. Nafady, Z.H.

- Ibupoto, Res. Chem. Intermed. 47, 1581 (2021); <https://doi.org/10.1007/s11164-020-04391-6>
- [23] J. Liu, Z. Shi, X. Li, J. Yang, J. Lang, J. Mater. Sci. 30, 13690 (2019); <https://doi.org/10.1007/s10854-019-01746-7>
- [24] M.G. Nair, M. Nirmala, K. Rekha, A. Anukaliani, Mater. Lett. 65, 1797 (2011); <https://doi.org/10.1016/j.matlet.2011.03.079>
- [25] I. Ne. Reddy, C.V. Reddy, J. Shim, B. Akkinapally, M. Cho, K. Yoo, D. Kim, Catal. Today 340, 277 (2020); <https://doi.org/10.1016/j.cattod.2018.07.030>
- [26] J. Wang, X.H. Sun, H. Du, Russ. J. Inorg. Chem. 65, 1111 (2020); <https://doi.org/10.1134/S0036023620070244>
- [27] H.A. Rafaie, N.A.A.M. Nazam, N.I.T. Ramli, R. Mohamed, M.F. Kasim, J. Aust. Ceram. Soc. 57, 479 (2021); <https://doi.org/10.1007/s41779-020-00541-6>
- [28] A. Nibret, O.P. Yadav, I. Diaz, A.M. Tadesse, Bull. Chem. Soc. Ethiop. 29, 247 (2015); <https://doi.org/10.4314/bcse.v29i2.8>
- [29] S. Irtiqa, A. Rahman, Russ. J. Phys. Chem. A 95, 1900 (2021); <https://doi.org/10.1134/S0036024421090260>
- [30] Powder Diffract. File, JCPDS-ICDD, 12 Campus Blvd., Newtown Square, PA 19073-3273, U.S.A. (2001).
- [31] W.S. Mohamed, A.M. Abu-Dief, J. Phys. Chem. Solids 116, 375 (2018); <https://doi.org/10.1016/j.jpcs.2018.02.008>
- [32] A.S. Morshedy, A.M.A.E. Nagger, S.M. Tawfik, O.I.S. El-Din, S.I. Hassan, A.I. Hashem, Egypt. J. Chem. 59, 609 (2016).
- [33] S. Coste, A. Lecomte, P. Thomas, T. Merle-Mejean, J.C. Champarnaud-Mesjard, J. Sol-Gel Sci. Technol. 41, 79 (2007); <https://doi.org/10.1007/s10971-006-0117-6>
- [34] V. Strelchuk, O. Kolomys, S. Rarata, P. Lytvyn, O. Khyzhun, C.O. Chey, O. Nur, M. Willander, Nanoscale Res. Lett. 12, 351 (2017); <https://doi.org/10.1186/s11671-017-2127-4>
- [35] S. Kumar, F. Ahmed, N. Ahmad, N.M. Shaalan, R. Kumar, A. Alshoabi, N. Arshi, S. Dalela, F. Sayeed, K. Kumari, Materials 15, 8184 (2022); <https://doi.org/10.3390/ma15228184>
- [36] S. Guo, Z. Du, S. Dai, Phys. Status Solidi B 246, 2329 (2009); <https://doi.org/10.1002/pssb.200945192>
- [37] T.B. Ivetić, M.R. Dimitrievska, I.O. Gúth, L.R. Dačanin, S.R. Lukič-Petrović, J. Res. Phys. 36, 43 (2012); <https://doi.org/10.2478/v10242-012-0012-0>
- [38] M.A. Hanif, Y.S. Kim, S. Ameen, H.G. Kim, L.K. Kwac, Coatings 12, 579 (2022); <https://doi.org/10.3390/coatings12050579>
- [39] Ö. Bilgili, J. BAUN Inst. Sci. Technol. 23, 50 (2021).
- [40] M. Samadi, M. Zirak, A. Naseri, E. Khorashadizade, A.Z. Moshfegh, Thin Solid Films 605, 2 (2016); <https://doi.org/10.1016/j.tsf.2015.12.064>
- [41] D. Commandeur, G. Brown, P. McNulty, C. Dadswell, J. Spencer, Q. Chen, J. Phys. Chem. C 123, 18187 (2019); <https://doi.org/10.1021/acs.jpcc.9b03609>
- [42] T.H. AlAbdulaal, V. Ganesh, M. AlShadidi, M.S.A. Hussien, A. Bouzidi, H. Algarni, H.Y. Zahran, M.S. Abdel-wahab, I.S. Yahia, S. Nasr, Materials 15, 3257 (2022); <https://doi.org/10.3390/ma15093257>
- [43] N.F. Djaja, R. Saleh, Mater. Sci. Appl. 4, 145 (2013); <https://doi.org/10.4236/msa.2013.42017>
- [44] X. Lv, T. Wang, W. Jiang, Ceram. Inter. 44, 9326 (2018); <https://doi.org/10.1016/j.ceramint.2018.02.145>
- [45] Z. Jiao, Z. Liu, Z. Ma, ACS Omega 4, 7919 (2019); <https://doi.org/10.1021/acsomega.9b00806>